3.1 INTERLAMINAR SHEAR STRENGTH AND TRANS-THICKNESS TENSILE STRENGTH OF CVI AND NITE SIC/SIC COMPOSITES — C. Shih, Y. Katoh, K. Ozawa, and L. Snead (Oak Ridge National Laboratory)

OBJECTIVE

The main objective of this work is to determine the trans-plane properties (interlaminar shear strength and trans-thickness tensile strength) of three different types of SiC/SiC composites. These properties are in general lower than the in-plane properties and thus are the potentially design-limiting factors for the composites in fusion applications.

SUMMARY

The interlaminar shear strength and trans-thickness tensile strength of three different SiC fiber reinforced SiC matrix composites were evaluated by double-notched shear test and diametral compression test, respectively, in a non-irradiated condition. One composite showed weak interlaminar shear strength (~10 MPa) because of poorly densified interlaminar matrix. When the interlaminar matrix are adequately densified, dominating failure locations become intra-fiber bundle with fiber/matrix debond, resulting in a higher interlaminar shear strength (~30 MPa). Trans-thickness tensile loading caused crack propagation initiating from fiber/matrix debond. The crack can easily grow with the uni-directional woven composite, resulting in a lower trans-thickness tensile strength of ~20 MPa. The crack growth was obstructed by the weave pattern in the 2D woven composites, resulting in a higher trans-thickness tensile strength of ~35 MPa.

PROGRESS AND STATUS

Introduction

SiC fiber reinforced SiC matrix composites are promising materials for fusion applications due to their excellent thermal, chemical and mechanical stability, their high radiation stability and low activation properties upon neutron irradiation [1-4]. The thermal physical and mechanical properties of near-stoichiometric SiC fiber/SiC matrix (SiC/SiC) composites have been vastly studied [2, 4-8]. Mechanical properties integrity of SiC/SiC composites at high neutron dose of up to 40 displacement per atom (dpa) and high temperature of up to 800°C has been demonstrated [9].

It is well known that two-dimensionally fiber-reinforced ceramic matrix composites (2D CMCs) have improved fracture resistance and damage tolerance in the in-plane direction. However, the trans-plane properties of these composites are generally much lower and need to be addressed. In the development of SiC/SiC composites as fusion materials, there is a lack of trans-plane mechanical properties studies compared to the vastly studied in-plane properties. Moreover, the trans-plane mechanical properties are believed to be related with the initial matrix cracking and the crack propagation behavior of these composites under in-plane loading.

Several test methods have been developed to study interlaminar shear strength (ILSS) including shot-beam flexure test [10], and double-notched shear (DNS) test [11-14]. The double-notch shear test was used in this study because small specimens can be used. This is crucially important for neutron irradiation studies since volume in the irradiation capsules are limited and

often expensive. Furthermore, this method can be applied to high temperature test relatively easily. However, it should be noted that the notches make the shear stress distribution in the specimen non-uniform [11, 13, 15].

The tensile strength perpendicular to the 2D plane of the plains weave composites or perpendicular to the fiber direction of the uni-directional composites is called the trans-thickness tensile strength (TTS). It is typically much lower than the tensile strength of the in-plane direction since the load is not shared directly onto the fibers but results in tensile loading across the weak fiber-matrix interface. Therefore, TTS is a potential design-limiting factor for certain applications. The TTS of 2D CMCs can be evaluated per ASTM C1468-06 at room temperature by utilizing adhesively bonded extenders to transfer the load. However, the applicability of this test is limited by the strength and the operation temperatures of the adhesive. The diametral compression test can evaluate TTS of disk-shaped samples without using adhesive and thus eliminate the strength and temperature constrains imposed by the adhesive [16-20].

In this report, the ILSS and TTS of SiC fiber reinforced SiC matrix composites were investigated and discussed at non-irradiated conditions at room temperature. The fracture surfaces were examined by an SEM.

Experimental

Three types of composites were used in this study. Their properties are summarized in Table 1. These composites cover 2 types of commercially available near-stoichiometric SiC fibers (Tyranno™ SA3 fiber and Hi-Nicalon™ Type-S fiber), 2 types of SiC matrix densification methods (chemical vapor infiltration and NITE process [21, 22]), and 3 different fiber architectures. In the chemical vapor infiltration (CVI) process, SiC based matrix is deposited from gaseous reactants on a heated SiC fiber preforms. The NITE process incorporates a fiber coating and the infiltration of nano-phase SiC power based mixed slurry to the coated fiber preform. The slurry contains oxides sintering aids. This process is finished by a pressure sintering at temperatures above the melting point of the transient eutectic phase [23, 24].

The fiber/matrix interphase was coated with a layer of pyrolytic carbon (PyC) of nominally either 150 or 500 nm thickness. The interphase coating and the CVI matrix densification were provided by Hypertherm High-Temperature Composite, Inc. (Huntington Beach, CA) using an isothermal isobaric CVI process. It should be noted that the HNLS/PyC150 composite used finer weave fabrics of 24 × 24 thread-per-inch with 250 filament yarns instead of regular 16 × 16 thread-per-inch with 500 filament yarns. This resulted in a more homogeneous composite structure and increased interlaminar porosity.

Table I. Summary of composite materials studied.

Designator	Reinforcement	Interphase	Matrix	Porosity (%)	Density (g/cm^3)
TySA/PyC150	Tyranno™-SA3 (7.5um) 2D Plain Weave, 17 × 17 tpi, 800 filament yarns, 0°/90°	PyC (150 nm)	CVI-SiC	18	2.58
HNLS/PyC150	Hi-Nicalon™ Type-S, 900 denier 2D Plain Weave, 24 × 24 tpi, 250 filament yarns, 0°/90°	PyC (150 nm)	CVI-SiC	23	2.40
NITE/PyC500	Tyranno™-SA3 (7.5um) Uni-directional	PyC (500 nm)	SiC-NITE process	<2	N/A

Interlaminar shear strength of the composites was determined at room temperature by a double-notched shear (DNS) test per ASTM C1292-00. The dimensions of the specimen are 20 mm (length) × 4 mm (width) × 2 mm (thickness) with a notch separation of 6mm.

Trans-thickness tensile strength of the composite materials was determined by a diametral compression test at room temperature [17, 20]. In the test, a diametral compressive load applied to a truncated disc specimen is converted to tensile load in the perpendicular orientation leading to failure in trans-thickness tension. The maximum tensile stress is

$$\sigma_T = \frac{2P}{\pi d t} \tag{1}$$

where d is the disk diameter, t the thickness, and P the compressive load. The specimens are 4 mm in diameter and 3 mm thick. Details of the test method can be found elsewhere [16, 25].

For the SA3/PyC150 composite, the compressive load is along one of the fiber directions so that the tensile stress is perpendicular to the weave plane. For the NITE/PyC500 composite, the compressive load is also long the fiber direction, leading to a tensile stress perpendicular to the fiber direction.

Microstructures of the fracture surfaces were examined with Hitachi S4800 field emission scanning electron microscope.

RESULTS AND DISCUSSION

Interlaminar shear strength (DNS test)

The interlaminar shear strength (ILSS) of different composites is shown in Table II. The in-plane tensile strength for the same material is also listed for comparison. Typical shear

stress vs. displacement curves are shown in Figure 1. HNLS/PyC150 composite showed a much lower ILSS of 10.7 MPa. The TySA/PyC150 composite showed a higher ILSS of 30.1 MPa. NITE/PyC500 composite exhibited the highest interlaminar shear strength of 37.5 MPa.

ILSS of similar 2D SiC/SiC composites (TySA fiber, 80 nm PyC interphase, CVI SiC matrix, 40% fiber volume fraction, 13% porosity) has been studied by Riccardi et al. using a short beam shear test [30] and a ILSS of 54 MPa was reported. The higher ILSS by the short beam shear test can be explained by several reasons: firstly, there are no planer regions of constant maximum shear stress in this test method [31]. Moreover, the compressive stress from the load application points constrains the crack opening, resulting in an overestimate of the 'true' ILSS [31].

Table II. LSS and TTS of SiC/SiC composites. In plane tensile properties are also listed for comparison. Numbers in the parenthesis indicate one standard deviation

Material	ILSS (MPa)	# of tests	TTS (MPa)	# of tests	In plane PLS[1] (MPa)	In plane UTS[2] (MPa)
HNLS/PyC150	10.7 (5.7)	8	-	-	83 (12) [28]	318 (22) [28]
TySA/PyC150	30.1 (3.3)	6	34.1 (3.2)	4	113 (19) [28]	274 (29) [28]
NITE/PyC500	37.5 (1.63)	4	21.4 (3.3)	4	142 (26) [29]	344 (25) [29]

[1]proportional limit stress

[2]ultimate tensile stress

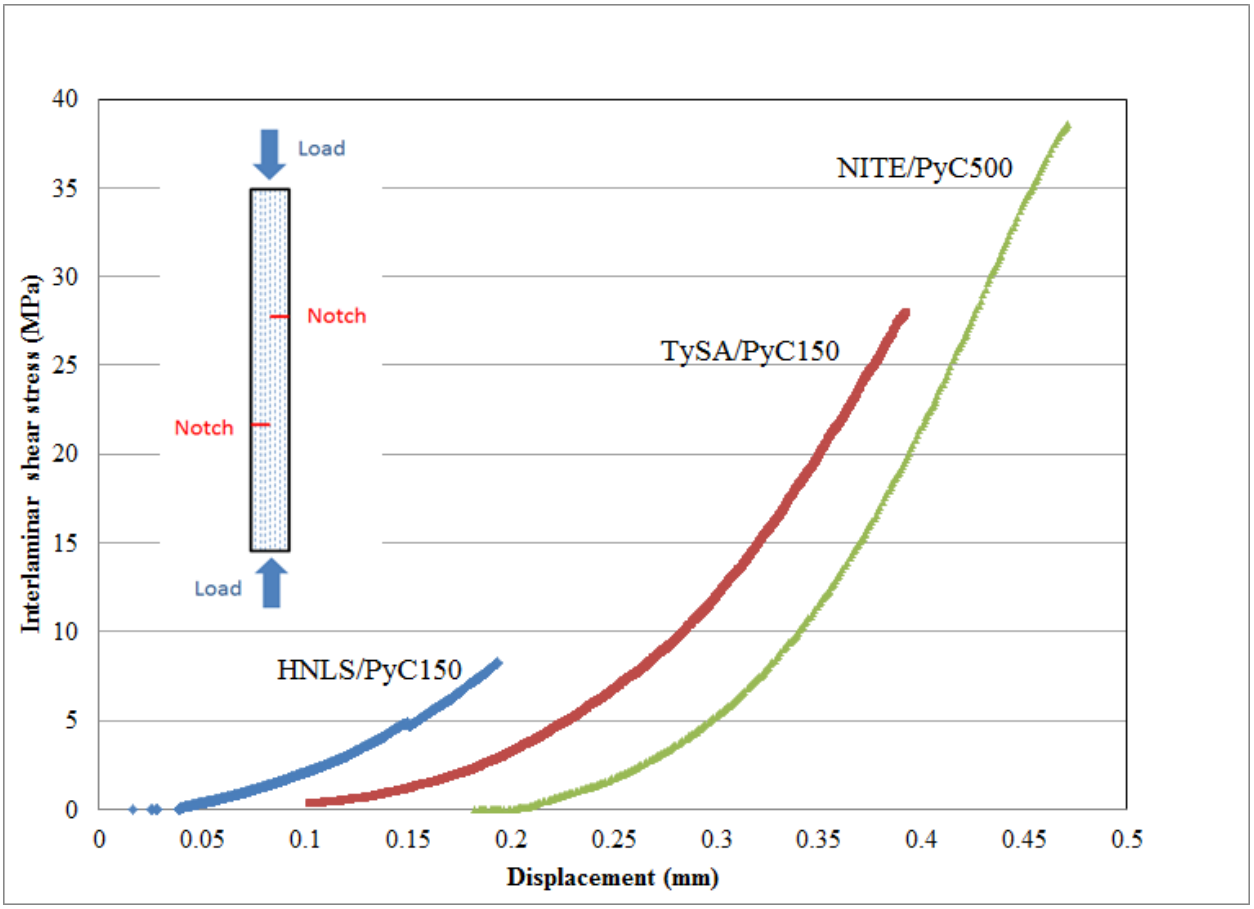

Figure 1. Tyrpical interlaminar shear stress vs. displacement curves in DNS tests. The horizontal positions are intentionally offset for better visibility.

SEM images of the fracture surface (Figures 2 and 3) of HNLS/PyC150 composites after DNS test showed a complete and an almost intact 2D interlaminar plane, indicating a failure between two fabric layers or true interlaminar failure. Apparently, the interlaminar layers are only connected by very limited areas, rendering very small interlaminar shear strength of 10.7 MPa. This is probably caused by the finer weave method that hinders the reactant gases from diffusing into the interlayer space. The areas where the inter layers were connected and broke by interlaminar shear can be clear seen in the SEM images (region 2 in Figure 2a and Figure 3).

Because of this failure mode, almost no fiber failures are involved with the composite failure. Further observations showed that the broken structures (region 2 in Figure 2a and Figure 3) are interlaminar matrices with fiber imprints. Some broken areas showed that the interlaminar matrices were pulled out, revealing the underneath bare fiber (Figure 3d). The blind or cavity regions between two adjacent tows can also be seen very clearly in Figure 2a (region 1). These blind regions didn't contribute directly to the low ILSS of the HNLS/PyC150 composite. Debond occurred between the SiC fiber and the PyC interphase coating (Figure 2d, e and f), leaving the PyC interphase attached with the matrix.

SEM images of a side of the HNLS/PyC150 composites after DNS test are shown in Figure 4. The interlaminar pores between plies can be seen very clearly. Two types of pores were observed. Region 1 in Figure 4a showed typical pores in 2D CVI SiC/SiC composites. Region 2 showed inter ply pores that were connected. This suggests an unusually poor bonding between fabric layers. The fracture occurred in the matrix between two adjacent plies, leaving a smooth fracture surface in the lateral images. This observation agrees with the fracture mode determined from the fracture surface image in Figure 2. Figure 4 also shows that the connected inter ply pores appear randomly in the HNLS/PyC150 composites, resulting in a larger scattering of composite ILSS with a coefficient of variation of 53%, as calculated from Table 2.

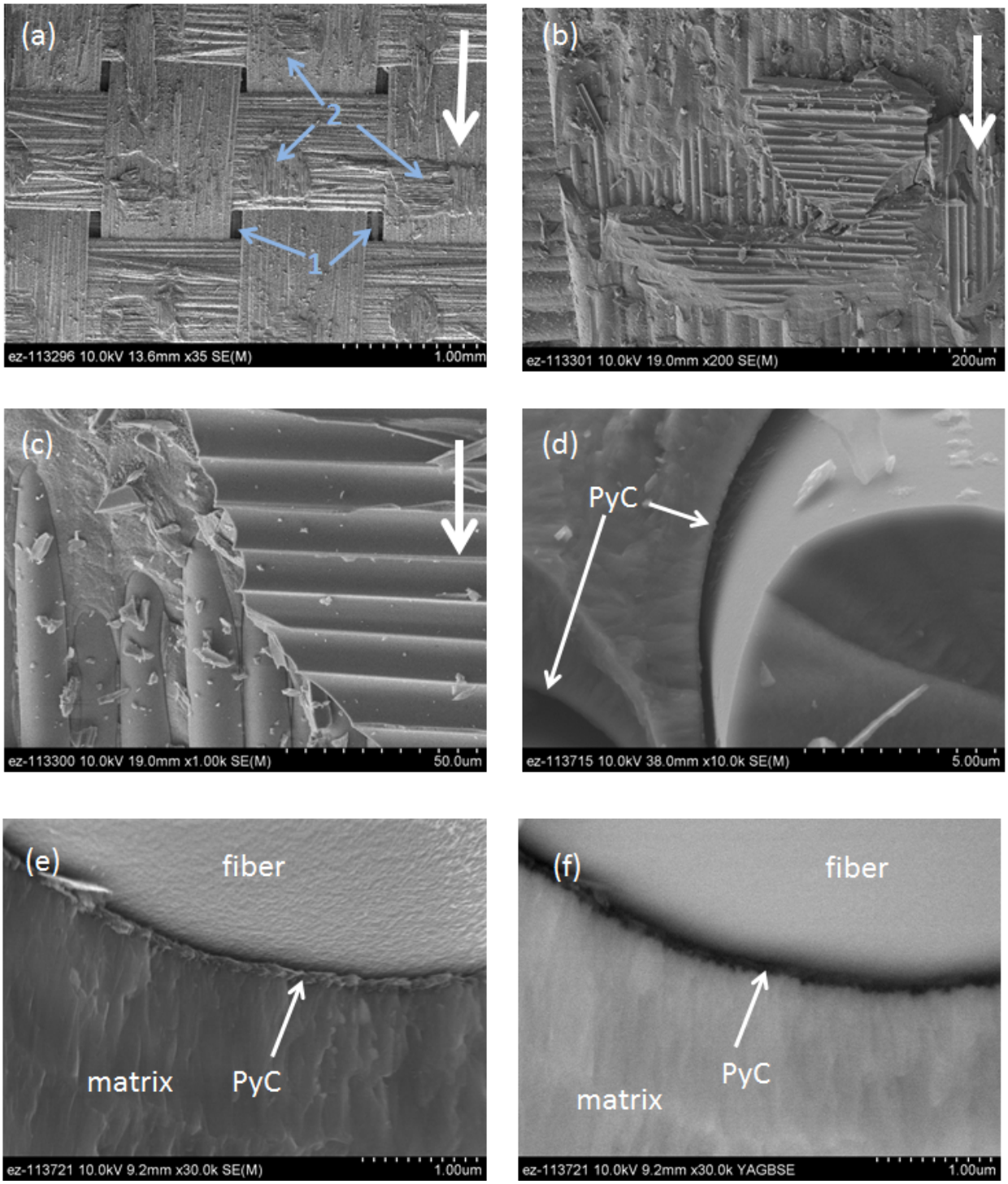

Figure 2. SEM Images of fracture surface of HNLS/PyC150 composites after double-notched shear test. Arrow represents the shear direction. Image (f) is the back scattered electron image of (e).

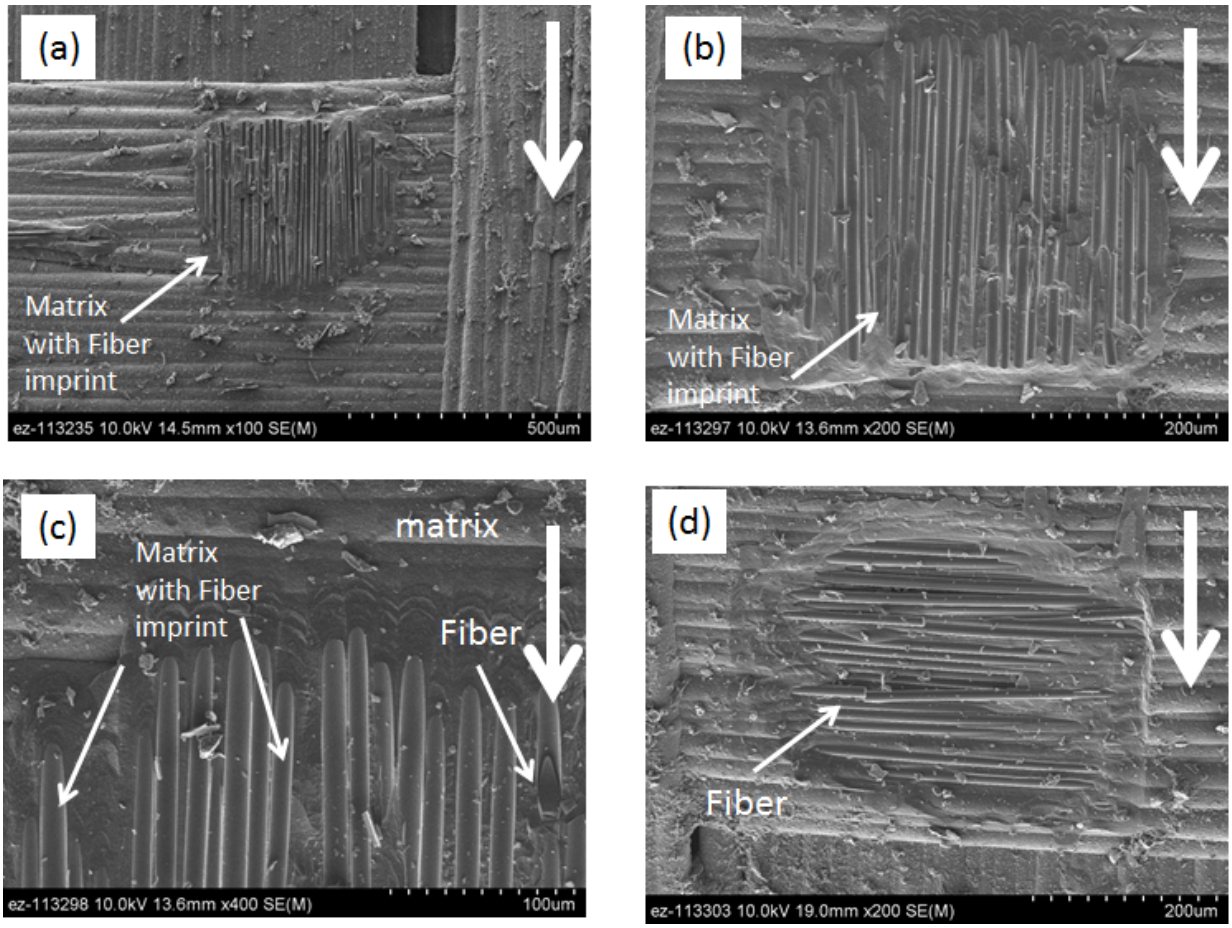

Figure 3. SEM Images of fracture surface of HNLS/PyC150 composites after double-notched shear test showing the matrix with fiber imprint (a, b, and c) and the revealed bare fibers (d). Arrow represents the shear direction.

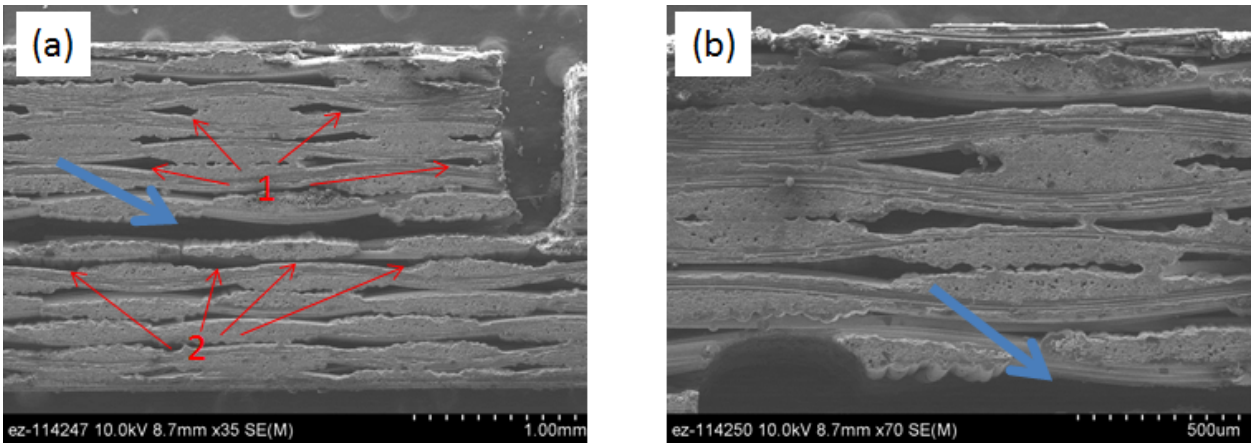

Figure 4. Lateral SEM Images of HNLS/PyC150 composites after double-notched shear test. Arrow indicates the fracture surface.

SEM images of TySA/PyC150 composites fracture surface (Figures 5 and 6) after DNS test show a 2D weave plane with damaged fiber tows. The lateral SEM images in Figure 7 show that the interlaminar layers are better densified by the CVI process as compared to the HNLS/PyC150 composites. Nonetheless, the images still show typical inter ply pores for 2D CVI SiC/SiC composites, i.e., the blind regions between fiber tows (inter-tow pores, region 1 in Figure 5a) and the non-densified space between adjacent layers (interlaminar pores, region 2 in Figure 5a). Since the interlayers are better densified, trans-thickness shear caused intra-bundle failure, revealing the intra-bundle SiC matrix and broken bare fibers (Figure 5a and Figure 7b). Some intra-bundle crack near the fracture surface can also be seen in Figure 7b (region 1). The intra-bundle SiC matrix is characterized by the small bumps. Failure inside the fiber tows rather than the interlaminar matrix rich regions suggests that the shear stress bearing capacity of the tows was lower than the interlaminar matrix rich regions when the interlaminar layers are adequately densified [30, 31]. This type of composite failure involves lots of fiber fracture and fiber/matrix debond and sliding, thus achieving higher interlaminar shear strength of 30.1 MPa. This intra-bundle failure mode results in a much lower scattering of ILSS with a variation coefficient of 11%. The inhomogeneity of the intra-bundle structure in the TySA/PyC150 composites appears to be much less than the structure inhomogeneity of the inter ply pores in the HNLS/Py150 composites. The broken tows appeared very rough, suggesting that slow crack growth alone the fiber matrix interphase is not predominating [30]. Debond occurred between the fiber and the PyC coating, leaving a thin layer of PyC coating on the matrix (Figure 6).

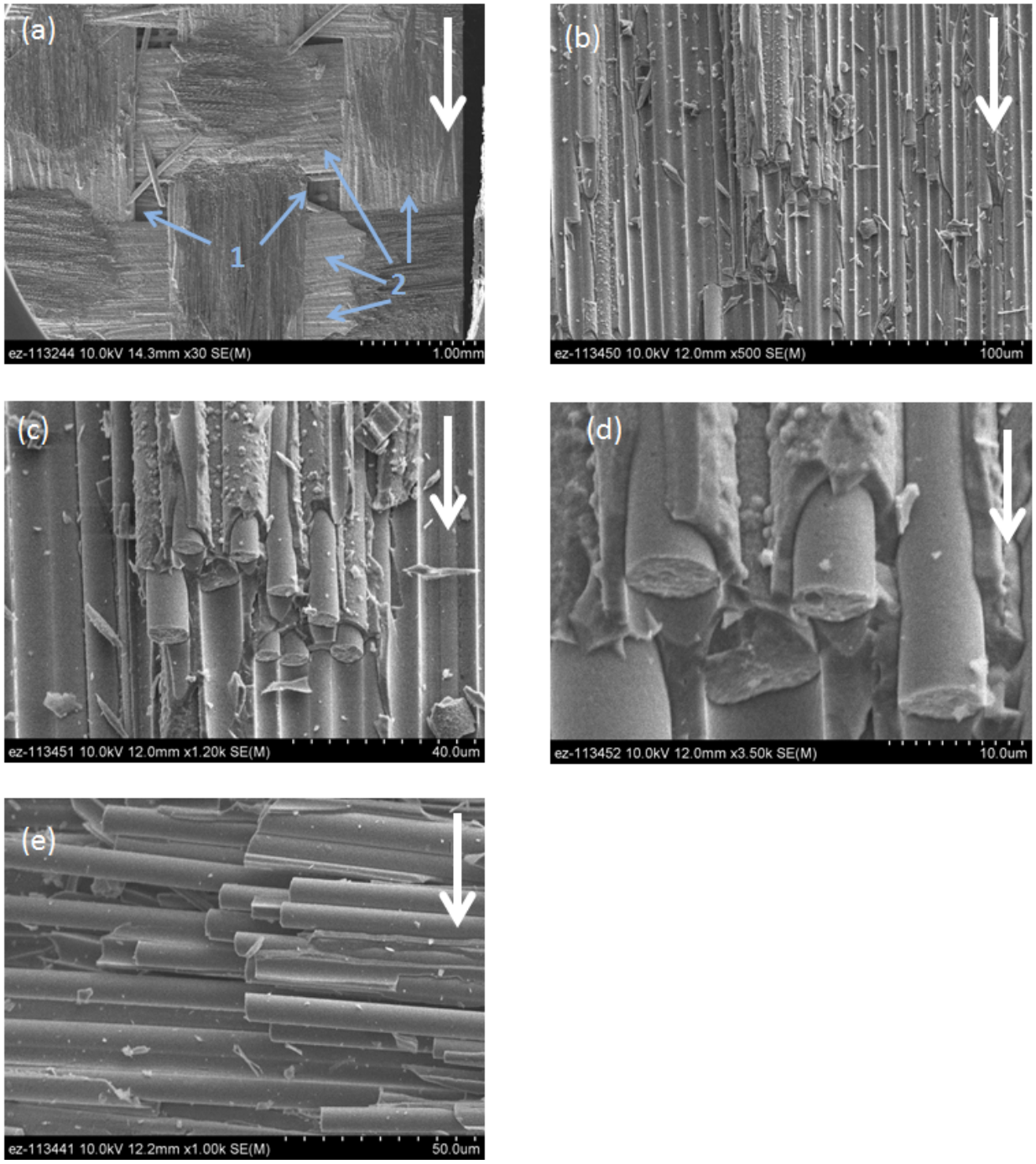

Figure 5. SEM Images of fracture surface of TySA/PyC150 composites after double-notched shear test. Arrow represents the shear direction.

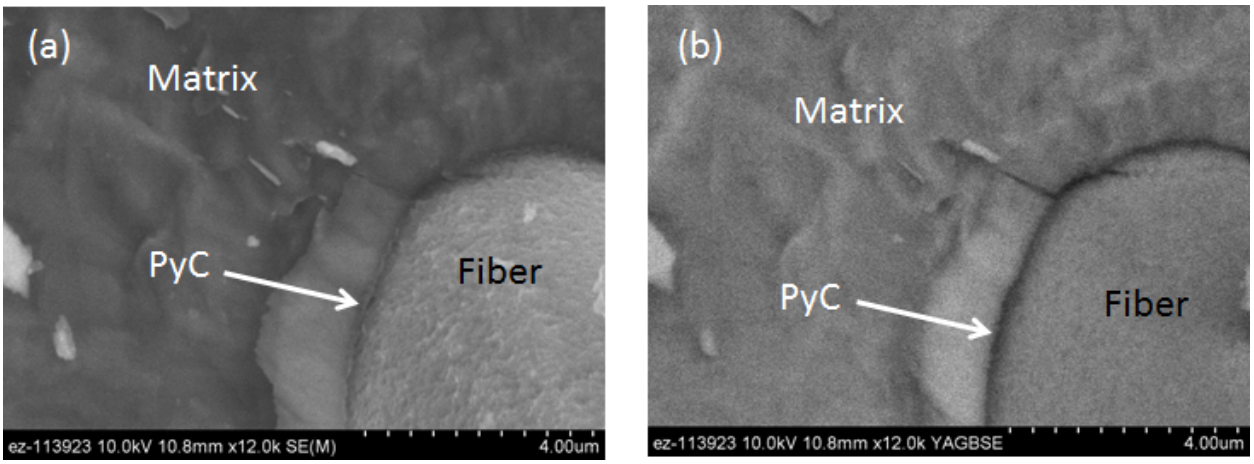

Figure 6. SEM Images of TySA/PyC150 composites after double-notched shear test that show the fiber, PyC interphase and the matrix. Image (b) is the back-scattered electron image of (a).

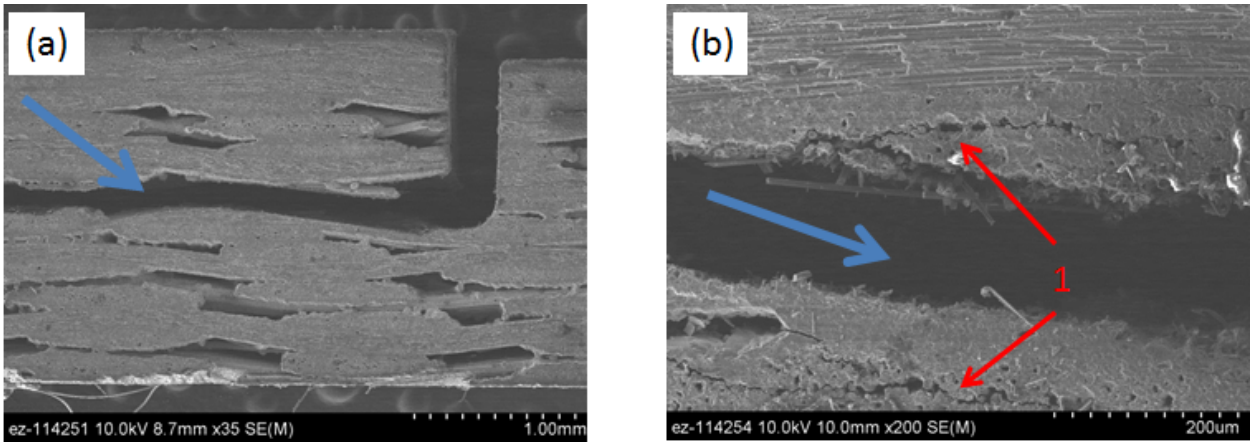

Figure 7. Lateral SEM Images of TySA/PyC150 composites after double-notched shear test. Arrow indicates the fracture surface.

Figure 8 shows the fracture surface of the NITE/PyC150 composite after DNS test. The sintering additives (white phase), the SiC matrix (grey phase) and the fiber with PyC coating (dark phase) can be readily distinguished from the back-scattered images. The NITE processed unidirectional composite appears to be relatively dense without large pores compared to the 2D weaved HNLS/PyC150 or TySA/PyC150 composites. The NITE/PyC500 composites have higher interlaminar shear strength because it didn't suffer from poor interlaminar densification like the 2D plain weaved CVI densified composites. The low porosity also results in very low ILSS scattering among the NITE/PyC500 samples, which have a variation coefficient of 4%.

Debond of NITE/PyC500 occurred between the PyC coating and the matrix, leaving most of the fibers still coated with the PyC interphase.

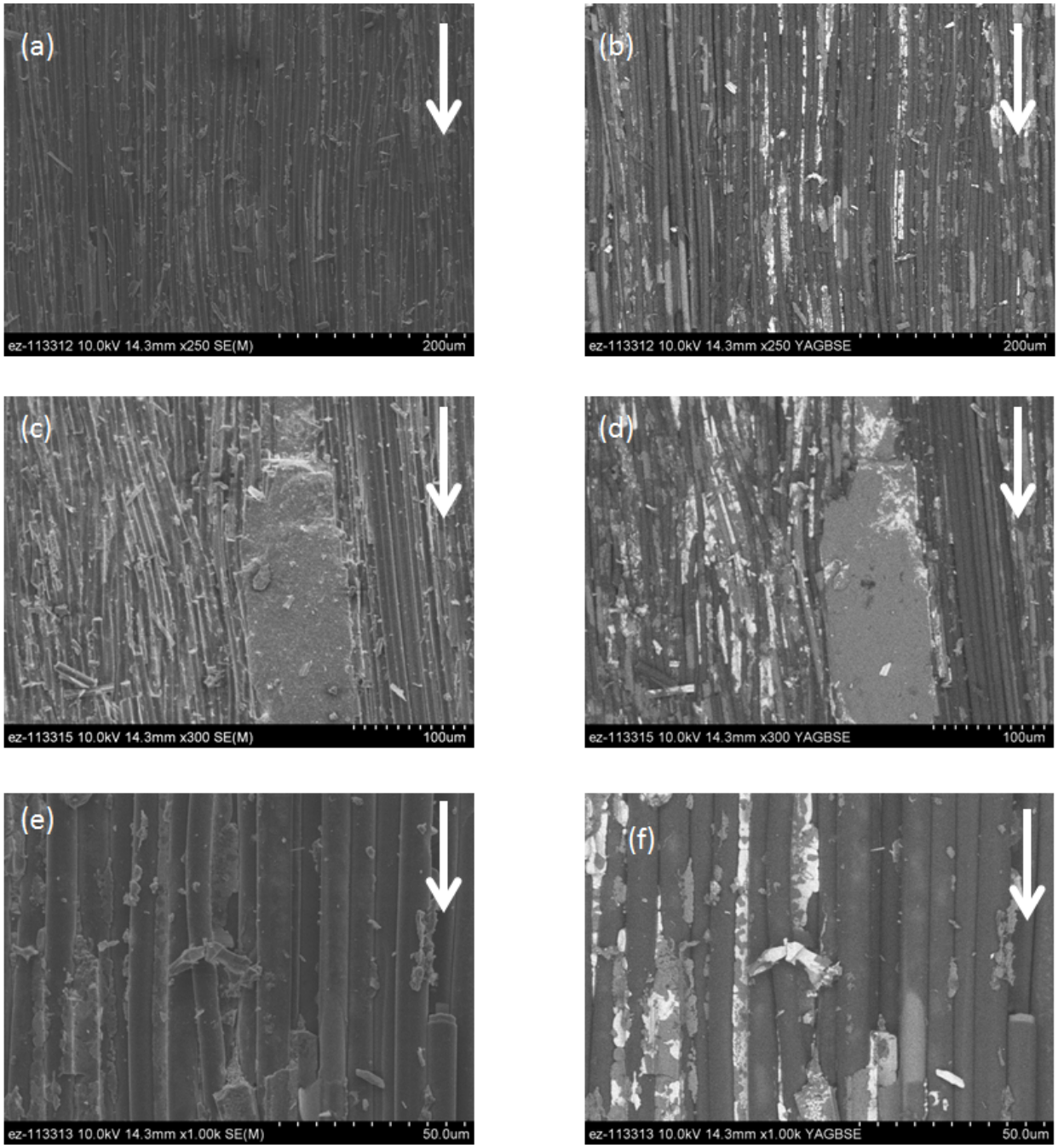

Figure 8. SEM Images of fracture surface of NITE/PyC50 composites after Double-notched shear test. (a), (c) and (e): secondary electron images, (b), (d) and (f): back scattered images. The arrow represents the shear direction.

Trans-thickness tensile strength (diametral compression test)

The Trans-thickness tensile strength of the composites is summarized in Table 2. SEM images of the fracture surface are shown in Figures 9 and 10 for TySA/PyC150 and NITE/PyC500 composites, respectively. TySA/PyC150 composite has a higher trans-thickness tensile strength than NITE/PyC500 in spite of the higher porosity of TySA/PyC150.

Nozawa et al. reported that without using a strain gauge, the diametral compression test would overestimate the TTS of SiC/SiC composites because a main crack initiated before the maximum load was reached [32]. Therefore, the "true" stress when the first major crack initiated in the specimens is smaller than the value reported here. TTS of similar 2D SiC/SiC composites has been reported by Riccardi et al. [26] by the adhesively bonded extender method and the reported TTS was only 7.6 MPa. The higher value obtained by the diametral compression method in this study might be partially caused by the overestimate of TTS by the diametral compression test. Another reason is that the effective volume of the diametral compression test is smaller than the effective volume of the adhesively bonded extender method, resulting in inherent higher measured TTS by the diametral compression test.

The fracture surface of TySA/PyC150 composite after diametral compression test showed a very uneven fracture plane (Figure 9). Failure appears to be intra-bundle and inter-ply with lots of fiber/matrix debond and fiber fracture. The intra-bundle fracture mode suggests that the trans-thickness tensile load bearing capacity of the intra-bundle matrix is lower than the inter-bundle matrix. This finding agrees with the low interlaminar shear load bearing capacity of the intra-bundle matrix discussed previously the 2D weave pattern prevented composite failure from just one direction of crack growth since tows form the other direction can still bear the trans-thickness tensile load. The final composite failure was caused by intra-bundle failure of fiber tows from both directions. Debond occurred between the fiber and the PyC, as shown in Figure 9d, reflecting stronger bonding between CVD SiC matrix and the PyC layer, as discussed previously for the same composite with interlaminar shear loading.

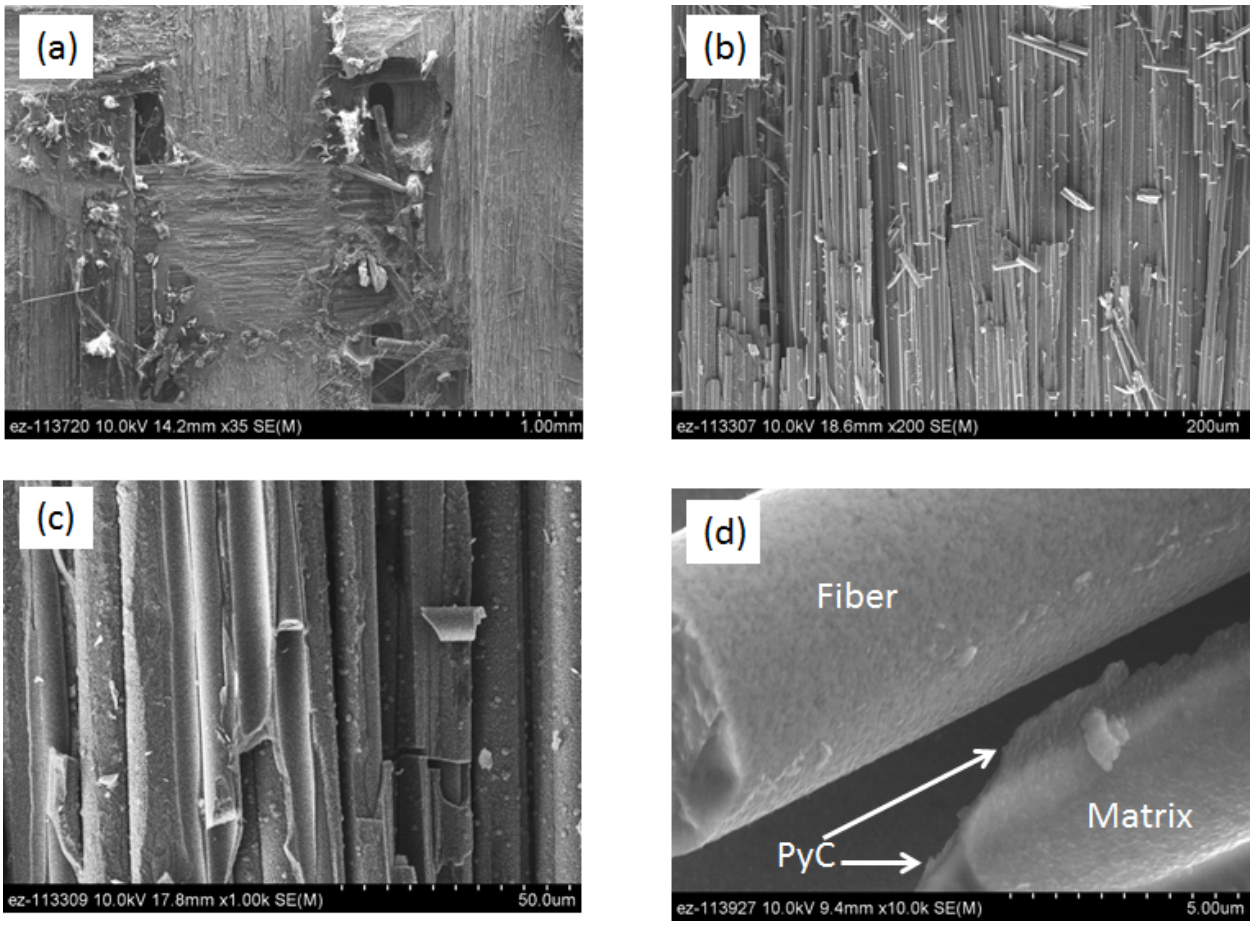

Figure 9. SEM Images of fracture surface of TySA/PyC150 composites after diametral compression test.

Fracture surface of NITE/PyC500 composite after diametral compression test (Figure 10) is flatter than the TySA/PyC150 composite because of the uni-directional weave architecture. Less fiber fracture is observed. On the contrary, it is observed that fibers are lifted by the trans-thickness tensile stress, revealing the matrix (with fiber imprint) underneath the fiber. Failure occurs mostly between the PyC coating and Matrix interphase so most of the fibers in the fracture surface still have a PyC coating. Even though the NITE/PyC500 composites have less porosity, the crack can grow along the PyC coating and the SiC matrix without much interference while subject to a trans-thickness tensile load, resulting in a smaller tensile strength (21.4 MPa).

Debond occurs mostly between the PyC coating and Matrix interphase so most of the fibers in the fracture surface still have a PyC coating. This agrees with the previous finding for the same composite under interlaminar shear loading.

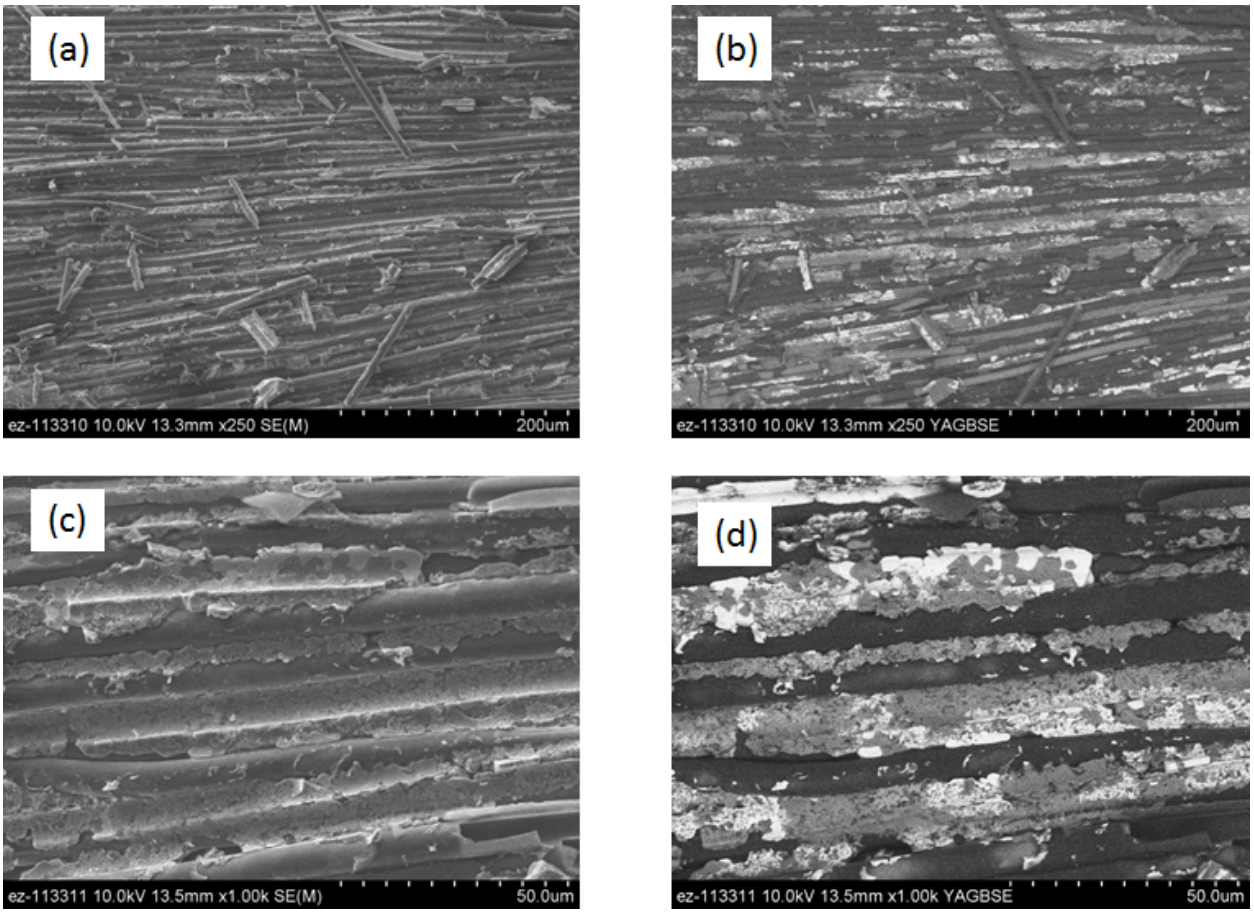

Figure 10. SEM images of fracture surface of NITE/PyC500 composites after diametral compression test. (a) and (c), secondary electron image; (b) and (d), back scattered electron image.

CONCLUSIONS

Interlaminar shear strength and trans-thickness tensile strength of different type of SiC fiber reinforced SiC matrix composites have been successfully evaluated with doubled notched shear test and diametral compression test respectively. HNLS/PyC150 composite has a low ILSS (10.7 MPa) because of poorly densified interlaminar matrix, resulting in interlaminar failure. TySA/PyC150 composite has a better densified interlaminar matrix, thus showing intra-bundle failure upon DNS test and a higher ILSS (30.1 MPa). The NITE/PyC500 composite showed the highest ILSS (37.5 MPa) because of its high density and the lack of interlaminar structure.

Upon diametral compression test, HNLS/PyC150 composites showed an intra-bundle fracture pattern with a TTS of 34.1 MPa. For the NITE/PyC500 composites, trans-thickness tensile stress caused the crack to grow along the PyC coating and the SiC matrix without much interference, resulting in a smaller TTS of 21.4 MPa. Debond occurred between the PyC coating and SiC fiber for the two CVI densified composites. For NITE densified composites, debond occurred between the PyC coating and the SiC matrix.

For 2D weave composites, both shear and tensile stress bearing capacities of the tows were lower than the interlaminar matrix, assuming the interlaminar matrix is adequately densified. The interlaminar mechanical properties of these SiC/SiC composites are much weaker than their in-plane properties. Whether the interlaminar properties will be the design limit of these materials need to be addressed for individual application.

REFERENCE

[1] R. J. Price and G. R. Hopkins, *J. Nucl. Mater.* **108** (1982) 732-738
[2] Y. Katoh and L. L. Snead, *J. ASTM Int.* **2** (2005) 12377
[3] G. Newsome, L. L. Snead, T. Hinoki, Y. Katoh and D. Peters, *J. Nucl. Mater.* **371** (2007) 76-89
[4] L. L. Snead, T. Nozawa, Y. Katoh, T. S. Byun, S. Kondo and D. A. Petti, *J. Nucl. Mater.* **371** (2007) 329-377
[5] L. L. Snead and S. J. Zinkle, *Nucl. Instrum. Methods Phys. Res. Sect. B-Beam Interact. Mater. Atoms* **191** (2002) 497-503
[6] Y. Katoh, L. L. Snead, C. H. Henager Jr., A. Hasegawa, A. Kohyama, B. Riccardi and H. Hegeman, *J. Nucl. Mater.* **367-370, Part A** (2007) 659-671
[7] T. Nozawa, Y. Katoh and L. L. Snead, *J. Nucl. Mater.* **367** (2007) 685-691
[8] Y. Katoh, L. L. Snead, T. Nozawa, S. Kondo and J. T. Busby, *J. Nucl. Mater.* **403** (2010) 48-61
[9] Y. Katoh, T. Nozawa, L. L. Snead, K. Ozawa and H. Tanigawa, *J. Nucl. Mater.* **417** (2011) 400-405
[10] K. T. Kedward, *Fibre Sci. Technol.* **5** (1972) 85–95
[11] O. Unal and N. P. Bansal, *Ceram. Int.* **28** (2002) 527-540
[12] O. Unal and N. P. Bansal, *Interlaminar shear strength of a unidirectional fiber-reinforced celsian composite by short-beam and double-notched shear tests*, in *25th Annual Conference on Composites, Advanced Ceramics, Materials, and Structures: A*. M. Singh and T. Jessen, Editors (2001) p. 585-595.
[13] M. M. Shokrieh and L. B. Lessard, *Appl. Compos. Mater.* **5** (1998) 49-64
[14] F. Sugiyama, K. Ogawa and T. Nishida, *J. Ceram. Soc. Jpn.* **104** (1996) 978-983
[15] N. J. J. Fang and T. W. Chou, *J. Am. Ceram. Soc.* **76** (1993) 2539-2548
[16] T. Hinoki, E. Lara-Curzio and L. L. Snead, *Evaluation of transthickness tensile strength of sic/sic composites*, in *27th International Cocoa Beach Conference on Advanced Ceramics and Composites: B*, W. M. Kriven and H. T. Lin, Editors (2003) p. 401-406.
[17] T. Hinoki, E. Lara-Curzio and L. L. Snead, *Fusion Science and Technology* **44** (2003) 211-218
[18] A. BrucknerFoit, T. Fett, D. Munz and K. Schirmer, *J. Eur. Ceram. Soc.* **17** (1997) 689-696
[19] M. K. Fahad, *J. Mater. Sci.* **31** (1996) 3723-3729
[20] M. Mellor and I. Hawkes, *Engineering Geology* **5** (1971) 173-&
[21] J. S. Park, A. Kohyama, T. Hinoki, K. Shimoda and Y. H. Park, *J. Nucl. Mater.* **367** (2007) 719-724
[22] Y. Katoh, S. M. Dong and A. Kohyama, *Fusion Eng. Des.* **61–62** (2002) 723-731
[23] Y. Katoh, A. Kohyama, T. Nozawa and M. Sato, *J. Nucl. Mater.* **329** (2004) 587-591
[24] S. M. Dong, Y. Katoh and A. Kohyama, *J. Am. Ceram. Soc.* **86** (2003) 26-32
[25] T. Hinoki, Y. Maki, A. Kohyama, E. Lara-Curzio and L. L. Snead, *Ceramic Engineering and Science Proceedings* **25** (2004) 65-70
[26] B. Riccardi, E. Trentini, M. Labanti, M. Leuchs, S. Roccella and E. Visca, *J. Nucl. Mater.* **367** (2007) 672-676
[27] S. T. Peters, *Handbook of Composites, 2nd edition*. 1998, Chapman & Hall, p. 790-791.

[28] Y. Katoh, K. Ozawa, T. Hinoki, Y. Choi, L. L. Snead and A. Hasegawa, *J. Nucl. Mater.* **417** (2011) 416-420
[29] Y. Katoh, *Unpublished data*
[30] S. R. Choi, R. W. Kowalik, D. J. Alexander and N. P. Bansal, *Compos. Sci. Technol.* **69** (2009) 890-897
[31] P. Brondsted, F. E. Heredia and A. G. Evans, *J. Am. Ceram. Soc.* **77** (1994) 2569-2574
[32] T. Nozawa, Y. Choi, T. Hinoki, H. Kishimoto, A. Kohyama and H. Tanigawa, *IOP Conference Series: Mater. Sci. Eng.* **18** (2011) 162011